Structural Study of Liquid Lithium Niobate by Neutron Diffraction Role of the Li Atom in the Clustering Near Solidification

P. Andonov, H. E. Fischer[a,*], P. Palleau[a], and S. Kimura[b]

CNRS-Laboratoire de Magnétisme et d'Optique de Versailles, Université de Versailles avenue des Etats-Unis Bat. Fermat, 78305 Versailles Cedex, France
[a] Institut Laue-Langevin, 156 X centre de tri, 38042 Grenoble Cedex, France
[b] National Institute for Research in Inorganic Materials, I-I Namiki, Tsukuba-shi, Ibaraki 305, Japan
* Current address: L.U.R.E. Bat. 209d, Boite postale 34, Centre Universitaire Paris-Sud, 91898 Orsay Cedex, France

Reprint requests to Mme. P.A; Fax: (1) 39 254 652; E-mail: lmov@physique.uvsq.fr

Z. Naturforsch. **56a,** 395–406 (2001); received February 12, 2001

The structure of liquid $LiNbO_3$ has been investigated by neutron diffraction using samples with different isotopic composition of lithium. The intensity scattered by these samples has been measured for momentum transfers $0.4\ Å^{-1} < Q < 17.1\ Å^{-1}$ and temperatures $1600\ K > T > 1500\ K$, which include the undercooling domain. From an analysis of the correlation functions $G_{ij}(r)$ of the atomic pairs Li–Li, Li–Nb, Li–O and their structural evolutions, given by $\Delta G_{i-j}(r) = G_{i-j}(r)_{1500} - G_{i-j}(r)_{1550}$ made with reference to the crystalline $LiNbO_3$ ferroelectric structure, it was possible to confirm a local ordering similar to that of the crystal. The presence of clusters (groupings of NbO_3 octahedra) is confirmed. Both regular and irregular NbO_6 octahedra are observed in the liquid near solidification. With its high mobility in the melt, the Li atom plays an important role in the clustering: the Li–O and Li–Nb bonds make possible the staking of four octahedra groups into clusters of eight octahedra or more. The Li–Li bonds join these groups. The diameter of the clusters is a least 22 Å in the undercooling regime.

Key words: Structure of Liquids; Neutron Scattering; Atomic Clusters; Liquid Lithium Niobate.

1. Introduction

Lithium metaniobate $LiNbO_3$ is one of the most interesting materials for optics owing to its electrooptical and non-linear optical properties [1]. Single crystals are synthesized from the liquid state by the Czochralski method on an industrial scale. So, in order to seek the best conditions for crystal synthesis, structure sensitive properties such as viscosity, density and surface tension have been measured [2, 3]. Near the melting point, anomalous behaviour has been detected, implying that some ordering clusters exist, probably formed by octahedral $\{NbO_6\}$ units in the melt [3–5] as observed in the crystal. The $LiNbO_3$ crystal is classified in the family of ilmenite. The ferroelectric phase, belonging to the rhombohedal system with the space group R3c, has been resolved by Abrahams et al. [6] and the thermal expansion of the interatomic bonds was studied by Megaw [7] and compared to those of other niobates belonging to the family of the perovskite-related structures. At the Curie point T_c just a few degrees below the melting point T_m ($T_c \cong 1460$ K and $T_m = 1526$ K), the paraelectric phase appears with the space group $R\bar{3}c$. Its structure has been recently studied by Boysen et al. [8, 9]. The progressive evolution of the local order was studied in situ from 1623 to 1490 K (including the undercooling domain), using high temperature X-ray diffraction [10] and high temperature neutron diffraction [11]. In this temperature domain the Nb atom remains octahedrally coordinated, and a local ordering similar to that of the crystal is described for the first neighbours. From structural analysis of the $LiNbO_3$ melt, carried out by means of Small Angle X-ray [12] and Small Angle neutron scattering [13], the presence of small clusters has been confirmed in the melt; their radius of gyration increases in the undercooled domain near solidification.

To explain the role of the Li atom in the formation of these macroclusters we have undertaken an experimental study by high temperature neutron diffraction using liquid $LiNbO_3$ samples having different isotopic ratios Li^6/Li^7.

2. Experimental Details

The samples were prepared in the NIRIM at Tsukuba (Japan). Li_2CO_3 and Nb_2O_5 powders of high purity (99.99%), and different isotopic enrichment in $^6Li/^7Li$

0932-0784 / 01 / 0500-0395 $ 06.00

Table 1. Characteristics of the studied samples.

Samples	Composition: ^{6}Li and ^{7}Li	Φ sample in mm
EI	7.42 ^{6}Li + 92.58 ^{7}Li	5 and 12
EII	24.17 ^{6}Li + 75.83 ^{7}Li	12
EIII	38.98 ^{6}Li + 61.02 ^{7}Li	12
EIV	52.61 ^{6}Li + 47.39 ^{7}Li	12
EV	66.82 ^{6}Li + 33.18 ^{7}Li	5
EVI	96.00 ^{6}Li + 4.00 ^{7}Li	5

for the lithium carbonate were mixed in congruent composition, pressed into cylindrical form and calcined at 1273 K for 5 h. The final rods of sintered $LiNbO_3$ so obtained are identical to those used for the growth of $LiNbO_3$ single crystals by the RF-heated Czochralski method. Six samples were obtained, as described in Table 1.

In view of its high corrosiveness, liquid $LiNbO_3$ has to be maintained under an oxidizing air atmosphere in a sealed platinium container. A change of composition was not observed during the experiment. An important density change exists between solid and liquid states ($d_{solid} \cong 4.63$ g cm^{-3} at 298 K and near T_m $d_{liquid} \cong 3.66$ g cm^{-3} at 1528 K), so the container dimensions (wall thickness 0.2 mm, height 100 mm and diameter 5 or 12 mm) are chosen to accommodate the volume expansion as well as to optimize the neutron diffraction experiment.

The experiments were carried out on the D4 spectrometer at the Institut Laue-Langevin in Grenoble (France). High temperature was obtained using a cylindrical vanadium heater equipped with radiation shields. Temperature control and monitoring were achieved via two Pt/Pt–Rh thermocouples in contact with the sample base. The melt temperature was controlled to ±3 K. Crucible and heater were placed in an evacuated bell-jar ($4 \cdot 10^{-6}$ torr) to minimize air scattering. The wavelength of the monochromatic beam {Cu (200)}, zero shift, stability and efficiency of the two ^{3}He multidectors and instrumental resolution were determined with great accuracy. The angular range of the measurement was within $2.50° \leq 2\Theta \leq 143.80°$ (2Θ = scattering angle). With a wavelength $\lambda = 0.700$ Å and $Q = (4\pi \sin \Theta)/\lambda$, the explored Q range extended from 0.39 to 17.10 Å^{-1}. The chosen beam sizes at the spectrometer centre (height = 50 mm and width = 10 mm when the diameter of sample $\Phi_{sample} = 5$ mm, or height = 40 mm and width = 17 mm when $\Phi_{sample} = 12$ mm) assured a uniform illumination of the sample volume. Under these beam conditions and given the sample scattering power, a complete angular scan of more than 900 points was achieved in 1.5 h with a counting precision of about 0.2%. Therefore the statistical errors were always small compared to the effects induced by temperature variation and by isotopic substitution.

A large undercooling domain ($\Delta T \cong 36$ K) has been observed previously [11], so the scattered intensities $I_s(2\Theta)$ from the $LiNbO_3$ melt were measured at four temperatures (1600, 1550, 1525 and 1500 K). For each sample the temperature was increased to 1625 K and maintained at this temperature during 20 mn, then the temperature was decreased to the desired value and the counting was started after a temperature stabilization time of 20 mn. The intensities scattered by an empty reference Pt cell of the same dimensions were always measured to study Pt recrystallization effects on warming and then on cooling, at each temperature chosen for the study of the melt.

The sample scattering $I_s(2\Theta)$ is calculated using the procedure previously described [14, 15] and applied to the raw intensities $I_{SCFB}(2\Theta)$, $I_{CFB}(2\Theta)$, and $I_{FB}(2\Theta)$, where the symbols S, C, F, and B represent the sample, container, furnace and background, respectively. Since we used a separate container for each sample and for the empty container, each having different intensities for the Pt bragg peaks (due to different size grains which were annelled to yet different sizes during sample heating), the previous standard procedure for subtraction of the empty container did not eliminate completely these peaks. Therefore we applied a 'by hand' gaussian fitting procedure to the Pt Bragg peaks, separately for the empty container and each sample, as described in [11]. In the case of a well isolated peak, the correction of the residual peak is then a straightforward subtraction of the two gaussian peak fits (sample + container and empty container). In the case of overlapping peaks the correction is more complicated. We had to fit the overlapping peaks with a known number of gaussian peaks for which the maxima positions are also known. We made successive attempts until a good correspondance with the measured curve was obtained. In this manner the Bragg peak subtraction, made directly on each diffractogramme, is as accurate as with the usual method in which the Bragg peaks are eliminated only after obtaining the partials $S_{ij}(Q)$, and we also obtained a corrected total $S(Q)$ for each sample.

The neutron intensities were corrected for background, furnace and container scattering and sample self-absorption using the values of the coherent scattering and absorption cross sections of the three elements as listed in [16, 17] and reported in Table 2, where the neutron scattering length of the Li atom is calculated us-

ing the values $b^6Li = +2.01$ and $b^7Li = -2.22$ fm. The contributions of multiple scattering, incoherent and inelastic scattering were subtracted. Then, the total interference function was obtained after normalization to the known scattering cross sections in the high-Q domain, where the oscillations of the diffracted intensities are small. The Placzek correction was applied from the effective mass $\langle M_{\text{eff}}\rangle$ given by

$$\frac{1}{\langle M_{\text{eff}}\rangle} = \sum \frac{c_i}{M_i},$$

where c_i is the concentration of each atomic isotope.

The value of $\langle M_{\text{eff}}\rangle$ varies from 13.7 to 14.6 according to the studied sample, since M_{Li} changes with the isotopic ratio $^6Li/^7Li$. The steepness of the rise in intensity at low-Q (due to small-angle scattering from the sample) prevents an accurate extrapolation of the thermodynamic limit $S(Q)$. A cross check of the data correction and normalization with the value of $S(0)$ obtained from the thermodynamic properties is therefore not possible.

3. Data Processing

The method of analysing the scattered intensity for non-crystalline systems is now well established. Only details relevant for the present work are recalled. Within the formalism of Faber and Ziman [18], generalized to a non-crystalline system with more than two kinds of atom, the total structure factor $S(Q)$ can be related to the partial structure factors $S_{ij}(Q)$ and the total scattering cross section per atom by $d\sigma/d\Omega(Q)$ as follows:

$$S(Q) = \left[\frac{d\sigma(Q)}{d\Omega} - (\langle b^2\rangle - \langle b\rangle^2)\right] \Big/ \langle b\rangle^2 = \sum_{i=1}^{m}\sum_{j=1}^{m} W_{ij}\, S_{ij}(Q). \quad (1)$$

In our case $m = 3$ and 1, 2, or 3 for Li, Nb or O, respectively. More explicitly, (1) can be written as

$$\begin{aligned} S(Q) = {} & (c_1^2\, b_1^2 / \langle b\rangle^2)\, S_{11}(Q) \\ & + (c_2^2\, b_2^2 / \langle b\rangle^2)\, S_{22}(Q) \\ & + (c_3^2\, b_3^2 / \langle b\rangle^2)\, S_{33}(Q) \\ & + (2\, c_1\, c_2\, b_1\, b_2 / \langle b\rangle^2)\, S_{12}(Q) \\ & + (2\, c_2\, c_3\, b_2\, b_3 / \langle b\rangle^2)\, S_{23}(Q) \\ & + (2\, c_3\, c_1\, b_3\, b_1 / \langle b\rangle^2)\, S_{31}(Q), \end{aligned} \quad (2)$$

Table 2. Values of the different coefficients used in the analysis and correction data. μ: Linear total absorption coefficients expressed in cm^{-1}, b_{coh}: Coherent scattering length expressed in fm, W_{ij}: Weights, expressed in %, of the partial functions defined in (1) and (2). The variation in $W_{\text{Nb–Nb}}$, $W_{\text{Nb–O}}$ and $W_{\text{O–O}}$ among the samples is due to the changing $\langle b\rangle^2$.

T (K)	μ Pt	μ V
1600	0.2514	0.13845
1550	0.2521	0.13859
1525	0.2524	0.13866
1500	0.2528	0.13873

T (K)	μ_{EI}	μ_{EII}	μ_{EIII}	μ_{EIV}	μ_{EV}	μ_{EVI}
1600	0.41195					5.19250
1550	0.41559	1.32302	2.13121	2.87403	3.64843	5.23823
1525	0.41730	1.32845	2.13995	2.88583	3.66340	5.25969
1500	0.41912	1.33424	2.14928	2.89840	3.67937	5.28290

	Nb	O	Li_{EI}	Li_{EII}	Li_{EIII}	Li_{EIV}	Li_{EV}	Li_{EVI}
b_{coh}	7.054	5.805	–1.903	–1.200	–0.575	0.000	0.600	1.835

Samples	$W_{\text{Li–Li}}$	$W_{\text{Nb–Nb}}$	$W_{\text{O–O}}$	$W_{\text{Li–Nb}}$	$W_{\text{Li–O}}$	$W_{\text{Nb–O}}$
EI	0.71	9.77	59.56	–5.27	–13.02	48.25
EII	0.27	9.19	56.01	–3.13	–7.72	45.38
EIII	0.06	8.72	53.12	–1.42	–3.51	43.03
EIV	0.00	8.31	50.65	0.00	0.00	41.04
EV	0.06	7.92	48.26	1.34	3.33	39.09
EVI	0.49	7.19	43.83	3.74	9.24	35.53

where

$$\langle b\rangle = \sum_{i=1,2,3}^{m} c_i\, b_i \quad \text{and} \quad \langle b^2\rangle = \sum_{i=1,2,3}^{m} c_i\, b_i^2$$

are the average coherent length and its mean square value, respectively; c_i and b_i are the atomic concentration and the coherent scattering length of the i^{th} element and W_{ij} is the pair contribution of atoms i, j or the weight of the partial factor $S_{ij}(Q)$ (see Table 2). The total pair correlation function is obtained by Fourier transformation of the reduced function to real space:

$$G(r) = \frac{2}{\pi}\int_{Q_{\min}}^{Q_{\max}} Q\,(S(Q) - 1)\sin(Qr)\,dQ, \quad (3)$$

which gives the radial function (RDF) as

$$\text{RDF}(r) = 4\pi r^2 \varrho_0 + rG(r) = 4\pi r^2 \varrho(r), \quad (4)$$

where ϱ_0 is the mean number density expressed in atoms per $Å^3$ and $\varrho(r)$ the atomic distribution function.

The exact coordination numbers are obtained by integration of the peaks of the partial radial distribution functions $\text{RDF}_{ij}(r)$. For instance, the atoms contained in

the n^{th} shell are given by

$$N_{ij}^{n} = c_j \int_{r_{ij\min}^{n}}^{r_{ij\max}^{n}} \mathrm{RDF}_{ij}(r)\,\mathrm{d}r, \tag{5}$$

where $r_{ij\min}^{n}$ and $r_{ij\max}^{n}$ are the lower and upper limits on the n^{th} shell defined by the minima of the $\mathrm{RDF}_{ij}(r)$; N_{ij}^{n} is the average number of atoms j in the n shell around an atom of type i choosen as origin, and the average distance between atoms i and j is given by

$$r_{ij} = \frac{(r_{ij_{\max}} + r_{ij_{\min}})}{2}$$

if the distribution can be approximated by a discrete Gaussian [19].

Different parasitic peaks appear in $G(r)$ after the Fourier transformation. The first ones, due to the limit of integration $Q_{\max}$, are easily suppressed. They are located on both sides of the main peak at a distance of about $5/2 \times \pi/Q_{\max}$. They are identified by changing the $Q_{\max}$ value or applying a damping coefficient to the interference function before the Fourier transformation. The second ones could be due to an inadequate subtraction of the intensity diffracted by the Pt container. If a residual Bragg peak subsists in $S(Q)$, it gives after the Fourier transformation some parasitic oscillations in $G(r)$. Their periodicity ($\Delta r = 2\pi/Q'$) and the position of the first oscillation ($\pi/2\,Q'$) depend on the position (Q') of this error in $S(Q)$. So it is possible to identify this residual peak and suppress it. It is also possible that inadequate subtraction of higher Q oscillations coming from the container would lead to artefacts in $G(r)$ after Fourier transform. These artefacts would be particularly evident in the partial $G(r)$ results. We have always confirmed that the peaks in our $G(r)$ and $\Delta G(r)$ results do not correspond to the Pt–Pt distances. Lastly, since the structural change in the liquid is principally studied from the difference of two $G(r)$ functions obtained at two different temperatures, some of these systematic errors are also cancelled in the subtraction.

4. Results

4.1 General Observations

Figure 1 shows that no particular changes in $I_s(2\Theta)$ are observed between 1600 and 1550 K. Therefore we present in this work only the structural evolution observed between 1550 and 1500 K. Note that the curves in the figures are often shifted vertically for clarity.

To extract the six partial functions $S_{ij}(Q)$, six different global structure factors $S(Q)$ with different W_{ij} contributions are necessary. A complete set of six experiments, obtained at 1550 and 1500 K, is shown in Figs. 2a and 2b, respectively. The $S_{ij}(Q)$ functions could have been deduced from the solution of the matrix for $[Y(Q)] = [A]\,[X(Q)]$. But several difficulties appear in the resolution of this system. The determinant $[A]$ has a very small value, the weight W of the contributions of the different pairs spreads widely (see Table 2). In addition,

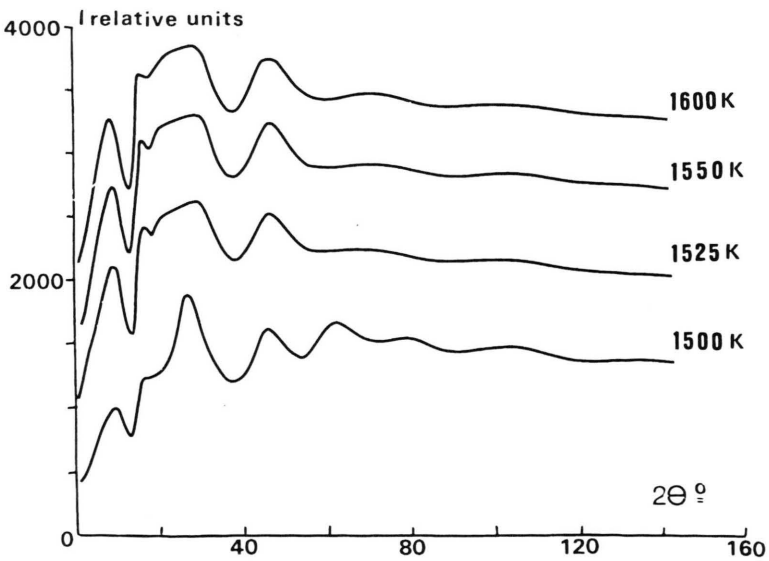

Fig. 1. Corrected intensities diffracted by sample I (natural Li) at 1600 and 1550 K (normal liquid), at 1525 K and at 1500 K (undercooled liquid). These curves are shifted vertically for clarity.

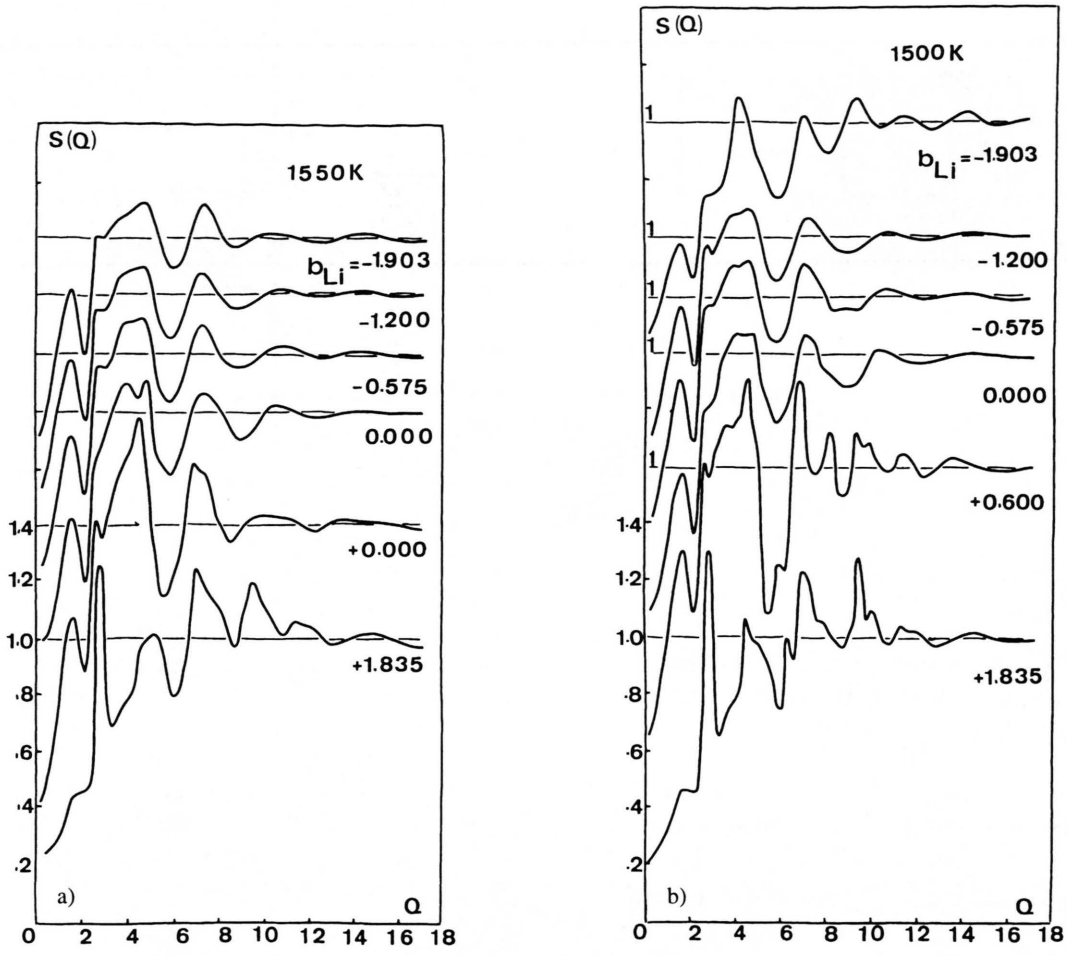

Fig. 2. a) Average structure factors $S(Q)$ of the samples I, II, III, IV, V, and VI at 1550 K (normal liquid); b) Average structure factors of the same samples at 1550 K (undercooled liquid).

the relative weights of the Nb–Nb, Nb–O and O–O contributions are all in almost the same ratio; so it is not possible to extract these three terms with a good accuracy. Nevertheless, we have made an exception for the partial $S_{\text{Li–Li}}(Q)$ factor. Using the change of sign observed in the contributions of Li–Nb and Li–O pairs in the samples E_I, E_{II}, E_{III} or E_V, E_{VI} and the no-contribution of Li–Li, Li–Nb and Li–O pairs in the sample E_{IV}, the direct determination of $S_{\text{Li–Li}}(Q)$ was possible without the resolution by the matrix form. The best regrouping of the experiments is given by

$$\{S(Q)_{EI} - 1.0770 \times S(Q)_{EIII} - 0.9117_5 \times S(Q)_{EIV} + S(Q)_{EVI}\}.$$

In this sum, all the pair contributions besides the Li–Li contribution can be neglected; this cancellation causes an error less than 0.10%. In this way the partial factors $S_{\text{Li–Li}}(Q)$ can be extracted with a total error less than 5%, even though the Li–Li contribution is the lowest of the six pair contributions.

4.2 Structural Evolution in the Undercooling Domain

The structural evolution versus temperature is described by the differences:

$$\Delta G_{ij}(r) = G_{ij}(r)_{1500} - G_{ij}(r)_{1550},$$

where $G_{ij}(r)_{1500}$ and $G_{ij}(r)_{1550}$ are the reduced radial distributions obtained at 1500 K (undercooled liquid) and 1550 K (normal liquid), respectively. In this T range the thermal expansion can be neglected because it is

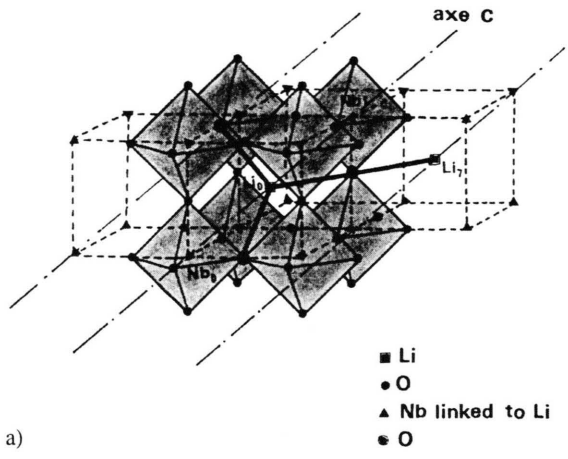

a)

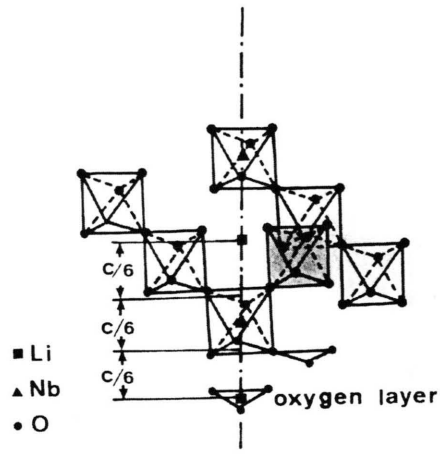

b)

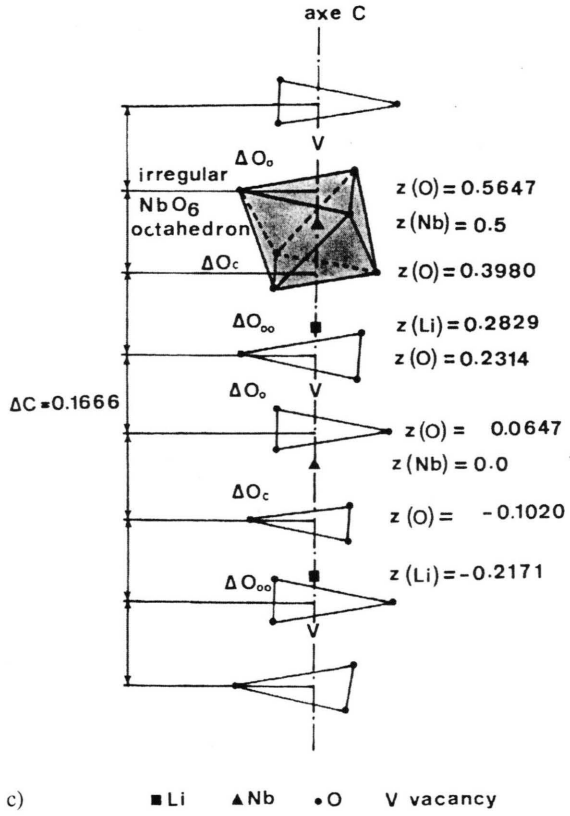

c)

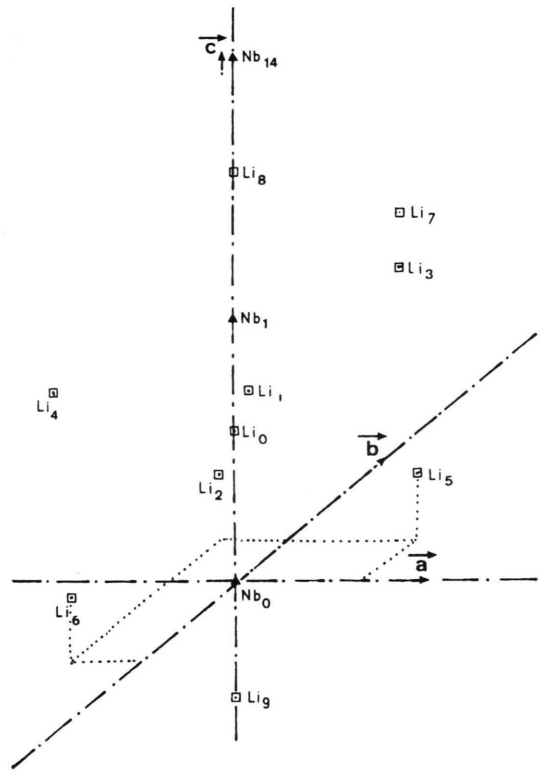

d)

small compared to the structural evolution. In the liquid near solidification it would be better to compare the atomic rearrangement with the high temperature paraelectric phase, in which the $Nb–O_6$ octahedron is assumed to be regular (see Figs. 3a and b and [8, 20, 21]), the first bonds Nb–O and O–O have been determined, and the high mobility of the Li atoms is confirmed [8, 9], but the atomic positions are not known in this high temperature phase. Some atomic bonds certainly differ from those in the ferroelectric phase (see Fig. 3c). The peaks observed for these differences are compared to the crystalline distances r_{ij} of the rhombohedral phase, calculated using the lattice parameters at room temperature [6] as follows: $a = b = 5.1483$ Å, $c = 13.8631$ Å,

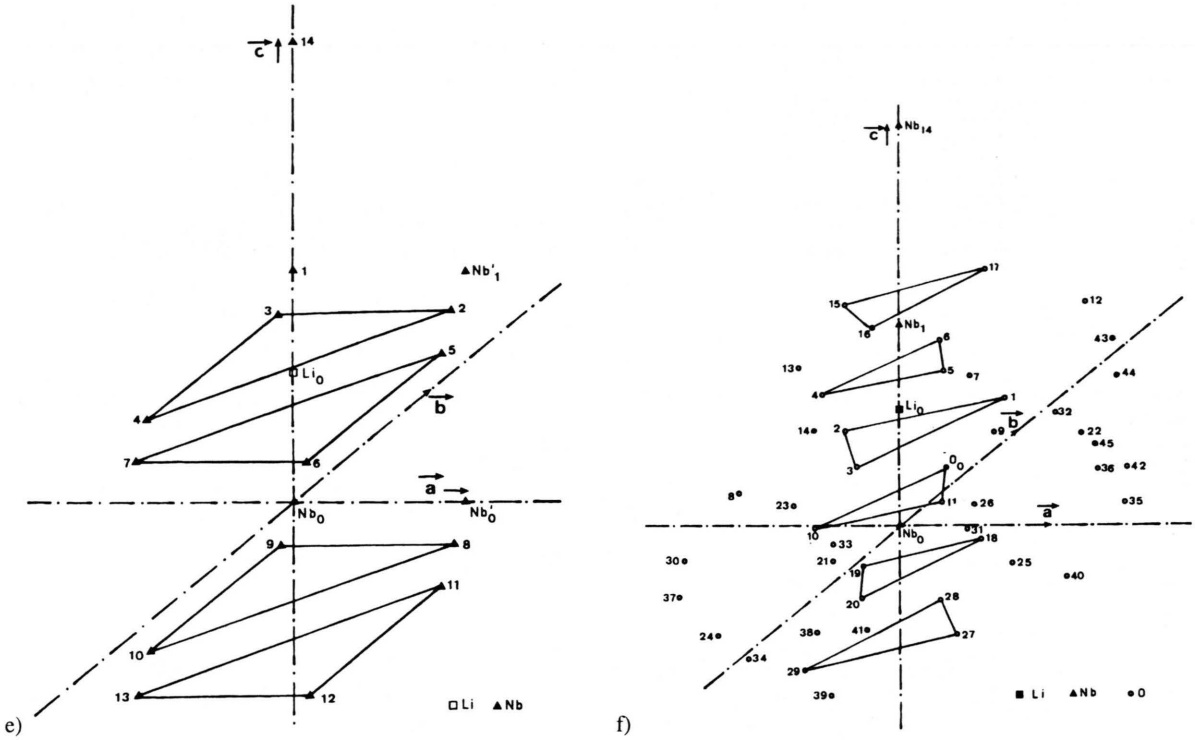

Fig. 3. Crystalline distributions: a) Framework of eight regular octahedra of oxygen atoms. b) Regular succession of Li and Nb atoms in the crystalline paraelectric phase. c) Sequence Nb, v, Li, Nb... (v = vacancy) along the threefold axis in the ferroelectric phase. d) Position of the neighbouring atoms Li in the crystalline ferroelectric phase. e) Position of the neighbouring atoms Nb in the crystalline ferroelectric phase. f) Position of the neighbouring atoms O in the crystalline ferroelectric phase.

with $\alpha = \beta = 90°$ and $\gamma = 120°$. The coordinates of the origin atoms are given by $x_0 \cdot a$, $y_0 \cdot b$ and $z_0 \cdot c$ with $x_0 = 0$, $y_0 = 0$, $z_0 = 0$, for the Nb_0 atom, $x_0 = 0$, $y_0 = 0$, $z_0 = 0.2829$ for the Li_0 atom, and $x_0 = 0.0492$, $y_0 = 0.3446$, $z_0 = 0.0647$ for the O_0 atom. The values of the crystalline distances r_{ij} are indicated on top of the curves $\Delta G_{ij}(r)$ by the line segments having a length proportional to the number of the atomic ij pairs in the crystal. The most probable distances r_{ij} present in the liquid are obtained by the positions of the maxima observed in the RDF (r) given by (4). It is more easy to determine these distances from the reduced functions $G_{ij}(r)$ or from their differences $\Delta G_{ij}(r)$ because the maxima appear more clearly in the curves. The values so obtained are weakly inferior to the real interatomic distances, and after this first determination we have to apply a correction evaluated from the RDF (r) curves. Another important fact is that the resolution obtained after the Fourier transformation is only $\Delta r = \cong 0.3$ Å with the experimental value of $Q_{max} = 17.5$ Å^{-1}.

Several neighbouring atoms will be considered in this study, so to simplify the text they are numbered, their coordinates in the ferroelectric phase are reported in the Tables 3a, b, and c, and their positions are shown in the Figs. 3d, e, and f for the Li, Nb and O atoms, respectively.

4.2. a) Evolution of the Li-Li Pairs

The partial factors $S_{Li-Li}(Q)$ are reported in Figs. 4a and b for 1550 and 1500 K, respectively. It is normal that the $S_{ij}(Q)$ curves are very structured because the sample is close to its solidification point. Their aspect indicates a significant atomic rearrangement near solidification in the undercooling domain. The partial $G_{Li-Li}(r)$ functions obtained by Fourier transformation are shown in Fig. 5 for the same temperatures, and the structural evolution $\Delta G_{Li-Li}(r)$ in Fig. 6. The first peak of $\Delta G_{Li-Li}(r)$ is narrow and centred at 3.3 Å; it corresponds to the first crystalline distance of the ferro-

Table 3. a) Coordinates of the first neighbouring Li atoms in the ferroelectric phase.

Number	x	y	z
0	0.0000	0.0000	0.2829
1	0.3333	–0.3333	0.4496
2	–0.3333	0.3333	0.1162
3	0.3333	0.6667	0.4496
4	–0.6667	–0.3333	0.4496
5	0.6667	0.3333	0.1162
6	–0.3333	–0.6667	0.1162
7	0.5000	0.5000	0.5647
8	0.0000	0.0000	0.7829
9	0.0000	0.0000	0.2171

Table 3. b) Coordinates of the first neighbouring Nb atoms in the ferroelectric phase.

Number	x	y	z
0	0.0000	0.0000	0.0000
0′	1.0000	0.0000	0.0000
1	0.0000	0.0000	0.5000
1′	1.0000	0.0000	0.5000
2	0.6667	0.3333	0.3333
3	–0.3333	0.3333	0.3333
4	–0.3333	–0.6667	0.3333
5	0.3333	0.6667	0.1667
6	0.3333	–0.3333	0.1667
7	–0.6667	–0.3333	0.1667
8	0.6667	0.3333	–0.1667
9	–0.3333	0.3333	–0.1667
10	–0.3333	–0.6667	–0.1667
11	0.3333	0.6667	–0.3333
12	0.3333	–0.3333	–0.3333
13	–0.6667	–0.3333	–0.3333
14	0.0000	0.0000	1.0000

Table 3. c) Coordinates of the first neighbouring O atoms in the ferroelectric phase.

Number	x	y	z	Number	x	y	z
0	0.0492	0.3446	0.0647	1	0.3825	0.3712	0.2314
2	–0.3712	0.0113	0.2314	3	–0.0113	–0.3825	0.2314
4	–0.2841	–0.3220	0.3980	5	0.3220	0.0379	0.3980
6	–0.0379	0.2841	0.3980	7	–0.0113	0.6175	0.2314
8	–0.6175	–0.6288	0.2314	9	0.6288	0.0113	0.2314
10	–0.3446	–0.2954	0.0647	11	0.2954	0.0492	0.0647
12	0.7159	0.6780	0.3980	13	–0.6780	0.0379	0.3980
14	–0.0379	–0.7159	0.3980	15	–0.3446	–0.0492	0.5647
16	0.0492	–0.2954	0.5647	17	0.2954	0.3446	0.5647
18	0.3220	0.2841	–0.1020	19	–0.2841	0.0379	–0.1020
20	–0.0379	–0.3220	–0.1020	21	0.0492	–0.6554	0.0647
22	0.6554	0.7046	0.0647	23	–0.7046	–0.0492	0.0647
24	–0.6780	–0.7159	–0.1020	25	0.7159	0.0379	–0.1020
26	–0.0379	0.6780	–0.1020	27	0.3825	0.0113	–0.2686
28	–0.0113	0.3712	–0.2686	29	–0.3712	–0.3825	–0.2686
30	–0.9508	–0.6554	0.0647	31	0.6554	–0.2954	0.0647
32	0.2954	0.9508	0.0647	33	–0.6780	0.2841	–0.1020
34	–0.2841	–0.9621	–0.1020	35	0.9621	0.6780	–0.1020
36	1.0492	0.3446	0.0647	37	–0.7046	–1.0492	0.0647
38	–0.6175	0.0113	–0.2686	39	–0.0113	–0.6288	–0.2686
40	0.6288	0.6175	–0.2686	41	0.3220	–0.7159	–0.1020
42	0.7159	1.0379	–0.1020	43	0.6288	1.0113	0.2314
44	0.9887	0.6175	0.2314	45	0.3220	1.2841	–0.1020

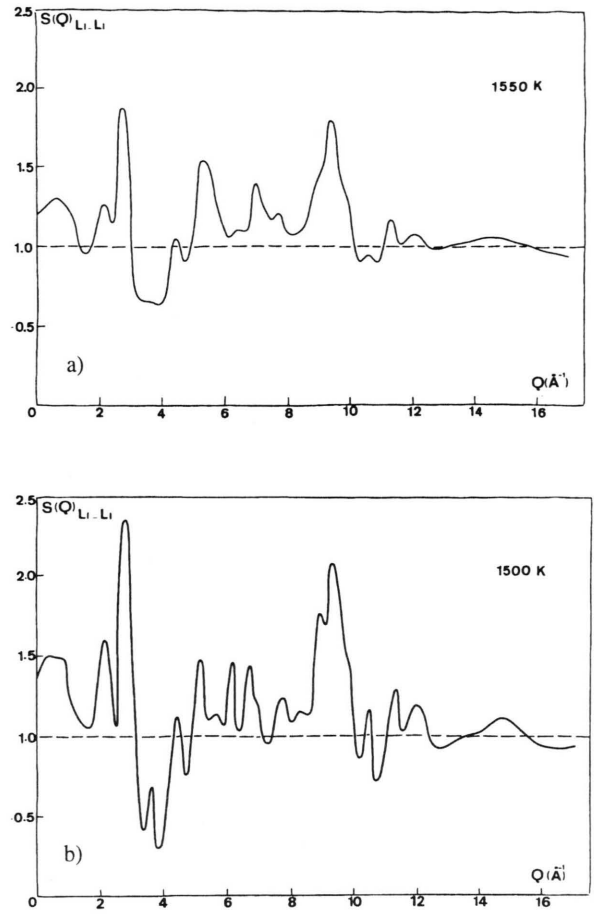

Fig. 4. Partial structure factor $S(Q)_{\mathrm{Li-Li}}$. a) Reported for 1550 K. b) Reported for 1500 K.

electric phase $r_{1\mathrm{Li-Li}} = 3.28$ Å (bonds between Li_0 and the two atoms Li_1 and Li_2) – (see Fig. 3d and Table 3a). The second experimental peak, centred at 4.4 Å, corresponds to the crystalline distance $r_{2\mathrm{Li-Li}} = 4.38$ Å (bonds between Li_0 and the four atoms Li_3, Li_4, Li_5, and Li_6). The previous two peaks are well separated, and each one corresponds to only one crystalline distance. Then we observe two peaks centred at 5.1 Å and at 5.4 Å. These values can be compared to two crystalline distances $r_{3\mathrm{Li-Li}} = 5.15$ Å and $r_{4\mathrm{Li-Li}} = 5.48$ Å. In the ferroelectric phase, these two distances represent the bonds between Li_0 and the Li_7 atoms located at the centres of the next frameworks of eight irregular NbO_6 octahedra. In the paraelectric phase (see Fig. 3a), only one distance represents these bonds, its value 5.40 Å is equal to the double of the first Li–O bond present in the elementary framework of regular eight octahedra. The

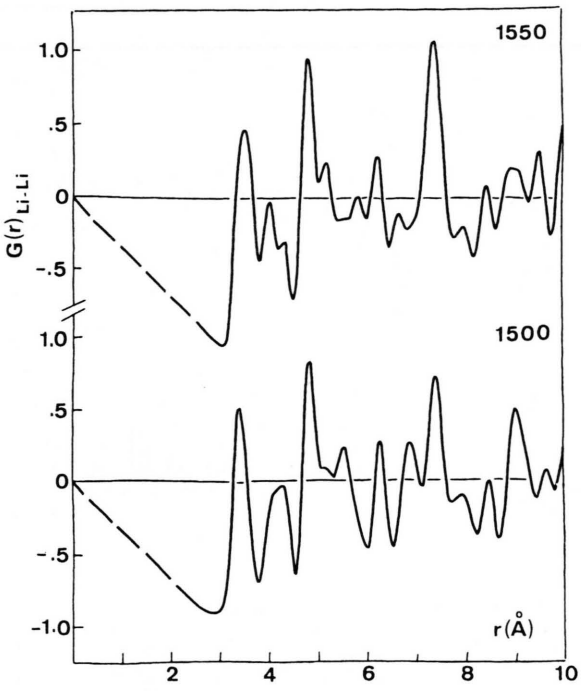

Fig. 5. Partial reduced distribution function $G_{Li\text{-}Li}(r)$ reported for 1550 and 1500 K.

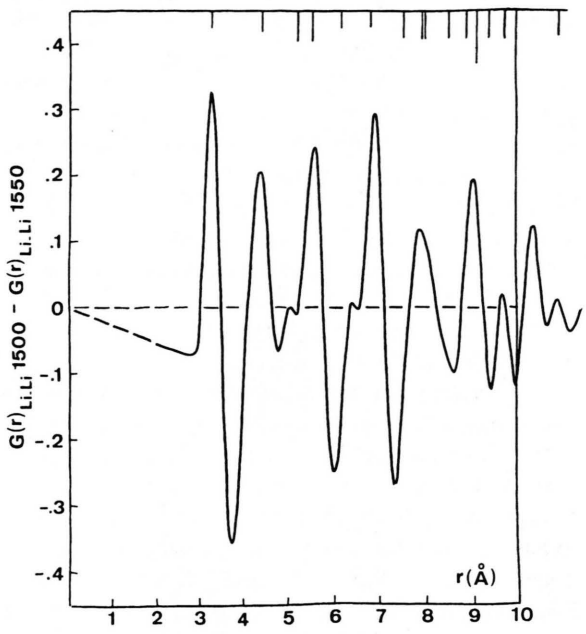

Fig. 6. Ordering evolution of the Li–Li bonds $\Delta\, G_{Li\text{-}Li}(r)$ between 1550 and 1500 K.

two experimental peaks observed in this r-domain confirm the presence of irregular NbO_6 octahedra in the liquid near solidification. The fact that the second one is much higher than the first one in the $\Delta G_{Li\text{-}Li}(r)$ indicates a rearrangement of the atoms to regular octahedra, like it was assumed in the crystalline paraelectric phase. The experimental peak observed at 10.90 Å (see the prolongation of the curve in the Fig. 6), confirms this rearrangement and a cluster formation. Aggregates are present in the liquid; they are constituted by four successive elementary frameworks at least in the direction $Li_0 \rightarrow Li_7$, so their diameter is equal to about 22 Å before solidification. The important peak located at 6.9 Å corresponds to the crystalline distance $r_{5\,Li\text{-}Li} = 6.93$ Å, given by the succession of Li atoms as it appears on the threefold axis (bonds between Li_0 and Li_8 or Li_9). Then successive experimental peaks are observed, but none of these represents only one crystalline distance. Nevertheless, a good agreement is always observed between their positions and the mean values of the crystalline distances regrouped due to the experimental resolution. The coordination numbers $N^n_{Li\text{-}Li}$ are determined from the $RDF_{Li\text{-}Li}(r)$ curves when the contributions can be well separated. We obtain for the first three contributions at 1550 and 1500 K, respectively: $N^1_{Li\text{-}Li} = 1.8$ and 2.0 ± 0.2, $N^2_{Li\text{-}Li} = 3.6$ and 4.0 ± 0.3 and $N^3_{Li\text{-}Li} = 2.5$ and 2.8 ± 0.3. These values have to be compared to the crystalline coordinations equal to 2 for the first $r_{1\,Li\text{-}Li}$ distances, 4 for the second ones $r_{2Li\text{-}Li}$, and 3 for the third ones $r_{3Li\text{-}Li}$, respectively. The experimental $N^3_{Li\text{-}Li}$ is somewhat inferior to the crystalline value, but this fact can be explained by the presence in the liquid near solidification of both regular and irregular NbO_6 octahedra. Consequently, a good agreement also exists for the coordination numbers. These results confirm the existence of aggregates in the liquid at 1550 K. Their size increases in the undercooling domain just before solidification (i.e. between 1530 K and 1500 K), and the atomic rearrangement moves towards crystalline order.

The contributions of the other atomic pairs have to be deduced from the resolution of a matrix form obtained by a system of five equations, since the partial interference function $S_{Li\text{-}Li}(Q)$ is now known. The value of the determinant is always weak, so the partial functions $S_{Li\text{-}Nb}(Q)$ and $S_{Li\text{-}O}(Q)$ are extracted with a weak accuracy. We, however, report the results relative to the Li–Nb and Li–O pairs because they confirm the previous description of the atomic Li rearrangement.

4.2. b) Evolution of the Li-Nb Pairs

The partial $G_{Li-Nb}(r)$ functions for 1550 and 1500 K, are reported in the Fig. 7, and the structural evolution $\Delta G_{Li-Nb}(r)$ in Fig. 8. The two first crystalline distances are $r_{1\,Li-Nb} = 3.01$ Å (bond between Li_0 and Nb_1) and $r_{2\,Li-Nb} = 3.05$ Å (bonds between Li_0 and the Nb triangle {2, 3, 4}), see the coordinates and the positions of the Nb atoms in the Table 3b and Fig. 3e, respectively. These distances cannot be separated in this work. They are represented by one large experimental peak present on both curves $G_{Li-Nb}(r)$. A large evolution is not observed in the undercooling domain. This peak is only more narrow at the low temperature and shifted to the higher r values. It is not possible to know which of the two bonds, Li_0–Nb_1 or Li_0–$Nb_{(2,\,3\,or\,4)}$, is the first one to be confirmed. The third crystalline distance $r_{3\,Li-Nb} = 3.38$ Å corresponds to the bonds between Li_0 the Nb triangle {5, 6, 7}. The experimental peak corresponding to this distance increases very much in the undercooling domain. The fourth crystalline distance $r_{4\,Li-Nb} = 3.92$ Å (bond Li_0 and Nb_0 (0, 0, 0)) is represented by the experimental peak centred at the same value. This peak increases between 1550 and 1500 K but remains broad with a trail on its right side. This fact could be explained by the large mobility of the Li atoms in the liquid. The next four crystalline distances cannot be separated in this work. Their successive values: $r_{5\,Li-Nb} = 5.96$ Å, $r_{6\,Li-Nb} = 5.99$ Å, $r_{7\,Li-Nb} = 6.09$ Å and $r_{8\,Li-Nb} = 6.16$ Å represent the distances between Li_0 and Nb_1' obtained from Nb_1 by the elementary 'a' periodicity. We observe only one experimental peak on the curve $\Delta G_{Li-Nb}(r)$ in this r-domain. Then the next crystalline distance is $r_{9\,Li-Nb} = 6.47$ Å (bond Li_0 and Nb_0' obtained from Nb_0 by the same elementary 'a' periodicity). Its value is different enough from the nearest ones to be extracted. We observe an experimental peak well separated in the curve $\Delta G_{Li-Nb}(r)$ at this value. The crystalline distance $r_{10\,Li-Nb} = 6.90$ Å (bonds between Li_0 and Nb triangle {8, 9, 10}) is also represented by a well defined experimental peak in the curve $\Delta G_{Li-Nb}(r)$. These two bonds are reinforced in the undercooling domain. Then a lot of successive crystalline distances having close values cannot be separated: $r_{11\,Li-Nb} = 7.90$ Å, $r_{12\,Li-Nb} = 7.98$ Å, $r_{13\,Li-Nb} = 8.03$ Å, and $r_{14\,Li-Nb} = 8.19$ Å. These distances are represented by the shoulder located at the left-hand side of the next experimental peak centred at 8.4 Å. This last peak could represent the crystalline distance $r_{15\,Li-Nb} = 8.61$ Å (always obtained by the elementary 'a' or 'b' periodicity); its maximum could be shifted to the lowest r-values due to the presence of the distances previously described. Other crystalline distances, such as $r_{16\,Li-Nb} = 9.05$ Å (bonds between Li_0 and the triangle Nb {1, 12, 13}), $r_{17\,Li-Nb} = 9.41$ Å and

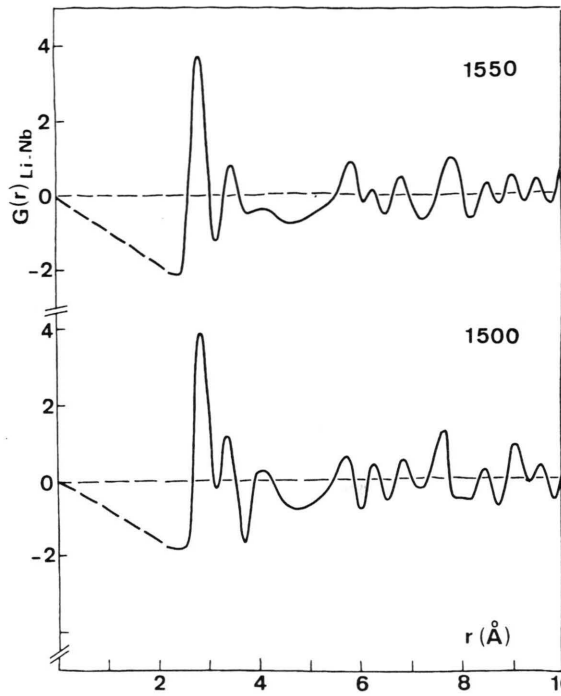

Fig. 7. Partial reduced distribution function $G_{Li-Nb}(r)$ reported for 1550 and 1500 K.

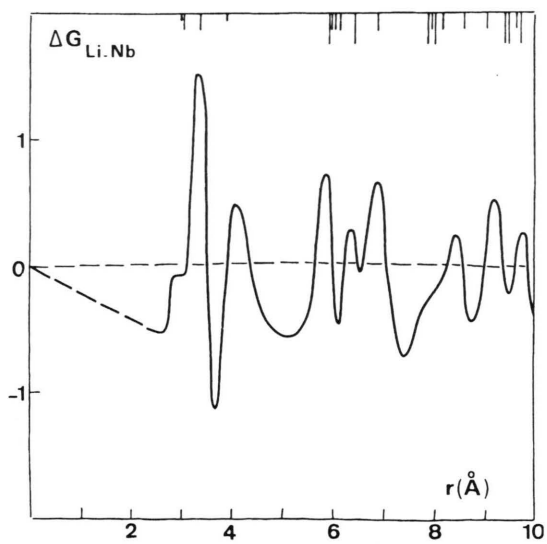

Fig. 8. Ordering evolution of the Li–Nb bonds $\Delta G_{Li-Nb}(r)$ between 1550 and 1500 K.

$r_{18\,Li-Nb} = 9.49$ Å (always obtained by the elementary 'a' periodicity), are represented by only one experimental peak located at 9.2 Å. The last experimental peak centred at 9.9 Å could represent the three crystalline distances: $r_{19\,Li-Nb} = 9.67$ Å and $r_{20\,Li-Nb} = 9.74$ Å, (bonds between Li_0 and the Nb atoms of the cell adjacent to the original cell) and $r_{21\,Li-Nb} = 9.94$ Å (bond between Li_0 and Nb_{14}, Nb_{14} corresponding to Nb_1 with a translation c/2). So, good agreement between experimental peaks and crystalline distances r_{Li-Nb} is always observed up to $r = 8$ Å, even when the interatomic distances are regrouped. Four of the previous interatomic distances r_{Li-Nb} can be separated. For these four well-separated Li–Nb contributions we have determined the coordination numbers N^n_{Li-Nb} from the $RDF_{Li-Nb}(r)$ curves at 1550 and 1500 K. These numbers are: $N^3_{Li-Nb} = 1.6$ and 2.3 ± 0.2 at 3.4 Å, $N^4_{Li-Nb} = 0.7$ and 1.1 ± 0.2 at 4.0 Å, $N^9_{Li-Nb} = 4.2$ and 5.5 ± 0.3 at 6.4 Å and $N^{10}_{Li-Nb} = 2.5$ and 2.8 ± 0.2 at 6.9 Å. The comparison of these values with the crystalline coordination numbers, respectively equal to $N^3_{Li-Nb} = 3$, $N^4_{Li-Nb} = 1$, $N^9_{Li-Nb} = 6$ and $N^{10}_{Li-Nb} = 3$, gives a good agreement with a rearrangement moving towards the crystalline order in going from 1550 to 1500 K.

4.2. c) *Evolution of the Li–O Pairs*

The partial $G_{Li-O}(r)$ functions for 1550 and 1500 K are reported in Fig. 9, and the structural evolution $\Delta G_{Li-O}(r)$ in the Fig. 10. The first peak in the $G_{Li-O}(r)$ curves shows a large shoulder on its right side and a deformation when the temperature decreases to 1500 K. This evolution is observed in the $\Delta G_{Li-O}(r)$ curve, which presents two well separated peaks in this r-domain; the first one corresponds to the first crystalline distance $r_{1\,Li-O} = 1.95$ Å (bonds between Li_0 and the three O atoms of the triangle {1, 2, 3}) and the second one to the crystalline distance $r_{2\,Li-O} = 2.30$ Å (bonds between Li_0 and the three O atoms of the triangle {4, 5, 6}) – (see the coordinates of the O atoms in Table 3c and their positions in Fig. 3f). The presence of these two r_{Li-O} distances indicates that the Li atom is not equidistant from the two adjacent O triangles as it was previously assumed in the high temperature crystalline phase. A distribution similar to the one observed in the ferroelectric phase is well confirmed in the liquid. The third crystalline distance $r_{3\,Li-O} = 3.21$ Å (bonds between Li_0 and the three O atoms of the triangle {7, 8, 9}) is represented in the two experimental $G_{Li-O}(r)$ curves obtained at 1550 and 1500 K. The fourth

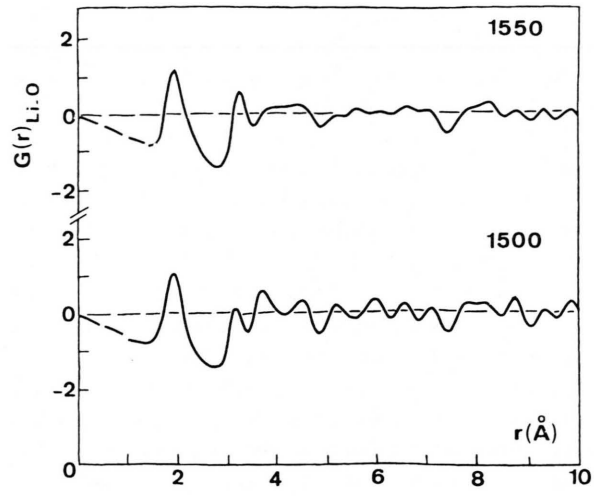

Fig. 9. Partial reduced distribution function $G_{Li-O}(r)$ at 1550 and 1500 K.

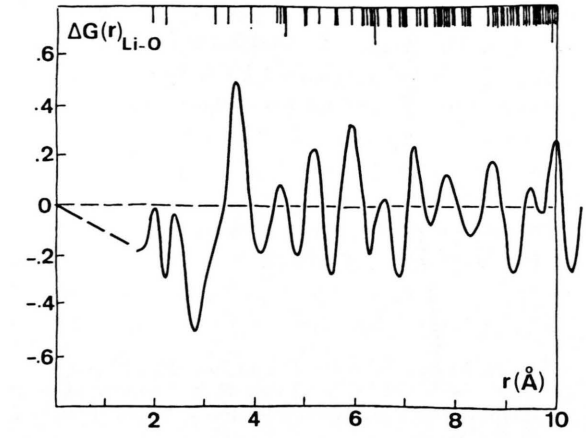

Fig. 10. Ordering evolution of the Li–O bonds $\Delta G_{Li-O}(r)$ between 1550 and 1500 K.

crystalline distance $r_{4\,Li-O} = 3.45$ Å (bonds between Li_0 and the three O atoms of the triangle {0, 10, 11}) is not well defined in the $G_{Li-O}(r)$ curves; only a large shoulder is observed on the left of a large experimental peak centred at 3.6 Å in the $\Delta G_{Li-O}(r)$ curve. This peak corresponds probably to the fifth crystalline distance $r_{5\,Li-O} = 3.93$ Å (bonds between Li_0 and the O atoms {12, 13, 14}); the high mobility of the Li atoms in the liquid could explain the width and the shift of this peak. The next experimental peaks of $\Delta G_{Li-O}(r)$ correspond to several crystalline distances. The peak centred at 4.5 Å represents the successive distances: $r_{6\,Li-O} = 4.46$ Å (bonds between Li_0 and the three O atoms of the triangle {15, 16, 17}), $r_{7\,Li-O} = 4.56$ Å, $r_{8\,Li-O} = 4.63$ Å

and $r_{9\,Li-O} = 4.69$ Å, (bonds between Li_0 and some O atoms which do not belong to the elementary O triangles stacked on the c axis). The peak centred at 5.2 Å represents the three crystalline distances $r_{10\,Li-O} = 5.00$ Å, $r_{11\,Li-O} = 5.10$ Å and $r_{12\,Li-O} = 5.29$ Å. It is not possible to determine which of these bonds are the first to be reinforced near solidification. From 6 Å on, the numerous crystalline distances Li–O are too close, we observe a succession of experimental peaks for which the positions are in good agreement with the mean values of several crystalline distances regrouped together due to the insufficient experimental resolution and also due to the small size of the clusters which bring about a broadening of peaks. Only the first three distances are well separated, and it has been possible to extract their coordination numbers from the $RDF_{Li-O}(r)$ curves. Their values at 1550 and 1500 K are, respectively: $N^1_{Li-O} = 2.5$ and 2.6 ± 0.2 for the mean $r_{1\,Li-O}$ distance equal to 1.9 Å, $N^2_{Li-O} = 2.7$ and 2.9 ± 0.2 for the mean $r_{2\,Li-O}$ distance equal to 2.4 Å (weakly superior to the crystalline distance) $N^3_{Li-O} = 2.1$ and 2.3 ± 0.2 for the mean $r_{3\,Li-O}$ distance equal to 3.2 Å. These values have to be compared to the crystalline coordinations numbers $N^1_{Li-O} = N^2_{Li-O} = N^3_{Li-O} = 3$. We also observe a good agreement with a rearrangement to crystalline ordering for the Li–O pairs.

We recall here that not Pt–Pt distance appears in our $\Delta G(r)_{ij}$ previously considered.

5. Conclusion

In undercooled molten $LiNbO_3$ at 1526–1500 K, using samples of different $^6Li/^7Li$ ratios, we have found a rearrangement toward regular octahedra, very similar to that present in the crystal phase. The Li atoms play an important role in the cluster formation: the Li–O bonds lead to staking of four NbO_6 octahedra, reinforcing their corner sharing. Thus elementary groups of eight octahedra are formed. The Li–Li bonds join these groups and thus induce the growth of clusters whose diameter in the undercooled regime we estimate to be at least 22 Å. The present investigations have confirmed and made more precise the conclusions of our previous studies of liquid $LiNbO_3$ (11, 12, 13).

Acknowledgements

The authors gratefully acknowledge financial support from the Special Coordination Fund for Promotion of Science and Technology granted for the study of the structure of clusters forming in melts and their influence on the crystal growth. The samples were prepared at the National Institute for Research in Inorganic Materials at Tsukuba, Japan. The neutron diffraction experiments were carried out at the Institut Laue-Langevin in Grenoble, France.

[1] A. A. Ballman, J. Amer. Ceram. Soc. **48,** 112 (1965).
[2] S. A. Bol'shvov, V. P. Klyuev, N. N. Lyapushkin, A. P. Liubimov, and S. A. Fedulov, Inorg. Mater. (USSR) **5,** 824–826 (1987).
[3] K. Shigematsu, Y. Anzai, S. Morita, M. Yamada, and H. Yokoyama, Japan J. Appl. Phys. **26,** 988–996 (1987).
[4] J. A. S. Ikeda, V. J. Fratello, and C. D. Brandle, J. Cryst. Growth **92,** 271–275 (1988).
[5] N. Niizeki, T. Yamada, and H. Toyoda, Japan J. Appl. Phys. **6,** 318–327 (1967).
[6] S. C. Abrahams, J. M. Reddy, and J. L. Berstein, J. Phys. Chem. Solids **27,** 997–1012 (1966). S. C. Abrahams, W. C. Hamilton, and J. M. Reddy, J. Phys. Chem. Solids **27,** 1013–1008 (1966). S. C. Abrahams, H. J. Levinstein, and J. M. Reddy, J. Phys. Chem. Solids **27,** 1019–1026 (1966).
[7] H. D. Megaw, Acta Crystallogr. **24a,** 583–588, 589–604 (1968).
[8] H. Boysen and F. Altofer, Acta Crystallogr. **50b,** 405–414 (1994).
[9] H. Lehnert, H. Boysen, F. Frey, and A. Hewat, Z. Kristallogr. Vol. 212, **10,** 712–719 (1997).
[10] K. Sugiyama, K. Nomura, Y. Waseda, P. Andonov, S. Kimura, and K. Shigematu, Z. Naturforsch **45a,** 1325–1327 (1990).
[11] P. Andonov, P. Chieux, and S. Kimura, J. Phys. Condens. Matter **5,** 4865–4876 (1993).
[12] P. Andonov, S. Kimura, and T. Sawada, J. of Non-Crystalline Solids **156–158,** 783–786 (1993).
[13] P. Andonov, S. Kimura, and P. Palleau, J. of Non-Crystalline Solids **205–207,** 163–167 (1996).
[14] H. Bertagnolli, P. Chieux, and M. D. Zeidler, Mol. Phys. **32,** 759–773 (1976).
[15] M. Maret, A. Pasturel, C. Senillou, J. M. Dubois, and P. Chieux, J. Physique **50,** 295–310 (1989).
[16] L. Koester and W. B. Yelon, Neutron Diffraction Newsletters, The neutron Diffraction Commission of the International Union of Crystallography (1983).
[17] V. F. Sears, Thermal neutron scattering lengths and cross-sections for condensed material research AECL Report 8490 (1984).
[18] T. E. Faber and J. M. Ziman, Phil. Mag. **11,** 153–173 (1965).
[19] W. R. Busing and H. A. Levy, Oak Ridge National Laboratory Report ORNL – TM-271 (1962).
[20] P. Andonov, P. Chieux, S. Kimura, and Y. Waseda, Z. Naturforsch **48a,** 955–964 (1993).
[21] P. Andonov, P. Chieux, and S. Kimura, Physica Scripta **T57,** 36–44 (1995).